iScience

Article

The molecular basis of pH sensing by the human fungal pathogen *Candida albicans* TOK potassium channel

Graphical abstract

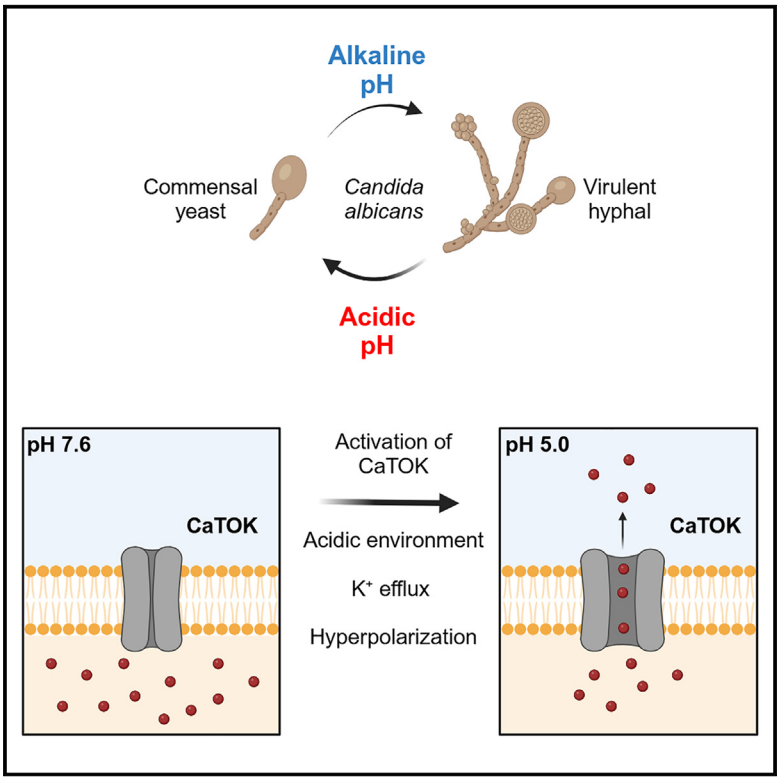

Highlights

- The *Candida albicans* TOK (CaTOK) K^+ channel senses extracellular pH
- Lowering extracellular pH augments CaTOK outward current and K^+ selectivity
- A tripartite network of residues comprises the complete CaTOK pH sensor
- CaTOK may help facilitate pH-dependent hyphal formation, a key virulence trait

Authors

Rían W. Manville, Claire L. Illeck, Anthony Lewis, Zoe A. McCrossan, Steven A.N. Goldstein, Geoffrey W. Abbott

Correspondence

abbottg@hs.uci.edu

In brief

Natural sciences; Biological sciences; Microbiology; Microbial physiology

Manville et al., 2024, iScience *27*, 111451
December 20, 2024 © 2024 The Author(s). Published by Elsevier Inc.
https://doi.org/10.1016/j.isci.2024.111451

CellPress

iScience

CellPress
OPEN ACCESS

Article

The molecular basis of pH sensing by the human fungal pathogen *Candida albicans* TOK potassium channel

Rían W. Manville,[1] Claire L. Illeck,[1] Anthony Lewis,[2] Zoe A. McCrossan,[3] Steven A.N. Goldstein,[4] and Geoffrey W. Abbott[1,5,*]

[1]Bioelectricity Laboratory, Department of Physiology and Biophysics, School of Medicine, University of California, Irvine, Irvine, CA 92697, USA

[2]School of Medicine, Pharmacy and Biomedical Sciences, University of Portsmouth, Portsmouth, PO1 2DT Hants, UK

[3]NIHR Evaluation, Trials and Studies Coordinating Centre (NETSCC), University of Southampton, Southampton, SO16 7NS Hampshire, UK

[4]Departments of Physiology & Biophysics, Pediatrics, and Pharmaceutical Sciences, Susan and Henry Samueli College of Health Sciences, University of California, Irvine, Irvine, CA 92697, USA

[5]Lead contact

*Correspondence: abbottg@hs.uci.edu

https://doi.org/10.1016/j.isci.2024.111451

SUMMARY

Two-pore domain, outwardly rectifying potassium (TOK) channels are exclusively expressed in fungi. Human fungal pathogen TOK channels are potential antifungal targets, but TOK channel modulation in general is poorly understood. Here, we discovered that *Candida albicans* TOK (CaTOK) is regulated by extracellular pH, in contrast to TOK channels from other fungal species tested. Low pH increased CaTOK channel outward currents (pKa = 6.0), hyperpolarized the voltage-dependence of TOK activation, and increased pore selectivity for K^+ over Na^+, shifting the reversal potential (E_{REV}) toward E_K. Mutating H144 in the S1-S2 extracellular linker partially diminished pH sensitivity, suggesting H144 forms part of the CaTOK pH sensor. Functional analysis of chimeras made with pH-insensitive *Saccharomyces cerevisiae* TOK and point mutants revealed that CaTOK V462 and S466 in the final transmembrane segment complete the pH-responsive elements. A tripartite network of residues thus endows CaTOK with the ability to respond functionally to changes in pH.

INTRODUCTION

First described in the baker's yeast *Saccharomyces cerevisiae*,[1] the two-pore domain, outwardly rectifying potassium (TOK) channel comprises eight membrane spanning domains and two pore loops (Figure 1A). Interestingly, despite being a tandem-pore potassium channel, TOK is evolutionarily distinct from two-pore domain potassium (K2P) channels in humans (Figure 1B), and shares no homologs in animals, plants, or insects. TOK channels have been cloned and characterized from several fungi, including the filamentous root fungus *Neurospora crassa* (NcTOK) and human fungal pathogens *Candida albicans* (CaTOK), *Aspergillus fumigatus* (AfTOK), and *Cryptococcus neoformans* var. *neoformans* (CnTOK).[2,3] A recent systematic review estimated that ~6.5 million people globally are affected by fungal infections, including 2.1 million with invasive *Aspergillus*, 1.8 million with chronic pulmonary aspergillosis, 1.5 million with candidemia, and 194,000 with cryptococcal meningitis.[4] Together, fungal infections contribute to more than 3.75 million deaths per year, with 2.5 million being directly attributable to the infection.[4] TOK channels have been posited to have potential as antimicrobial targets, with several studies proposing their activation by small molecules or peptides as a possible molecular switch for instigating programmed cell death and apoptosis.[5–10] However, little is known about pharmacological and environmental factors that modulate TOK channels from human fungal pathogens. Previously, *S. cerevisiae* TOK (ScTOK) was shown to be insensitive to changes in extracellular pH, a trait postulated to have evolved to facilitate regulation of intracellular homeostasis of electrogenic ions despite inhabiting environments with different and changing pH levels.[11,12] Whether insensitivity to extracellular pH is a trait shared by other TOK channels, notably those cloned from human fungal pathogens, has remained undetermined. Here, we report that CaTOK channel function is highly sensitive to pH and is CaTOK-specific among the species tested. Extracellular acidification potentiates CaTOK channel currents, induces a negative-shift in the voltage dependence of activation, and changes the ion selectivity of the conduction pore, hyperpolarizing the resting membrane potential. Using chimeras and site-directed mutagenesis, we reveal that the molecular mechanism underpinning CaTOK channel sensitivity to external pH is a sensor comprised of a residue in the extracellular S1-S2 linker and S8 residues contributing to the second pore domain.

This is an open access article under the CC BY-NC-ND license (http://creativecommons.org/licenses/by-nc-nd/4.0/).

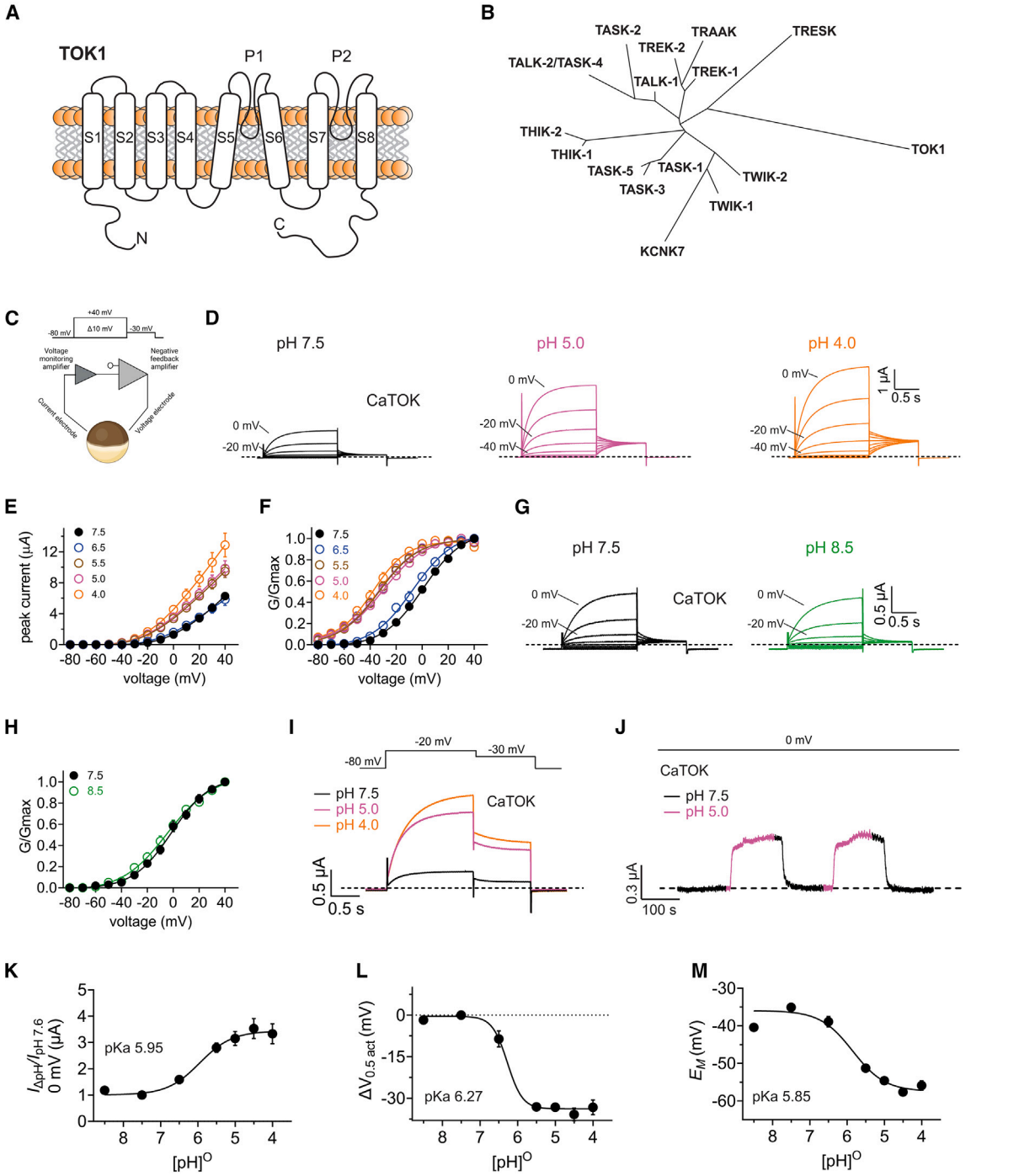

Figure 1. Extracellular acidification significantly potentiates CaTOK channel currents and induces a hyperpolarizing shift in the voltage-dependence of activation

Data are represented as mean ± SEM.

(A) Cartoon depicting the topology of fungal TOK channel with eight pore spanning transmembrane domains (S1-S8) and two pore loops (P1 and P2).

(B) Dendrogram depicting the evolutionary relationship between human tandem-pore domain potassium (K2P) channels and TOK1.

(C) Schematic of two electrode voltage-clamp setup and the *Xenopus* oocyte expression system used to measure TOK channel biophysical properties. Upper inset: voltage protocol used to generate current-voltage relationships. Created with BioRender.com.

(D) Averaged traces for CaTOK channels as indicated, expressed in oocytes in the presence of pH 7.5, pH 5.0, and pH 4.0. Scale bar upper right; n = 8–26 per group.

(legend continued on next page)

RESULTS

CaTOK channel activity is stimulated by extracellular acidification

From a starting point of pH 7.5 (standard physiological buffer), CaTOK outward currents were significantly increased by lowering the bath pH < 6.5, with a 2-fold increase observed at +40 mV at pH 4.0 (Figures 1D and 1E). Concurrently, CaTOK currents were also significantly increased at negative membrane potentials in response to increasingly acidic pH (Figures 1D, 1E, S1A and S1B), shifting the midpoint voltage dependence of CaTOK channel activation ($V_{0.5act}$) by −30.25 mV at pH 5.0 (from −1.81 ± 1.55 mV at pH 7.5 to −32.33 ± 1.33 mV at pH 5.0) (Figure 1F).

In contrast, shifting from pH 7.5 to a more alkaline pH (pH 8.5) did not alter CaTOK activity or $V_{0.5act}$ (Figures 1G and 1H). Figure 1I shows an example of the pH dependence of CaTOK currents at a single voltage (−20 mV) for direct comparison. Wash-in and washout experiments at 0 mV revealed immediate, robust potentiation of CaTOK channel outward currents upon wash-in, immediately reversible upon commencing washout (Figure 1J).

We next sought to establish the pKa of the effect, by measuring CaTOK channel current at 0 mV in a range of extracellular pH values. There was a 3-fold difference in peak current between pH 4.0 and pH 8.5. The resulting pH-response curve revealed a pKa of 6.0 ± 0.2 (Figure 1K). Likewise, fitting the $V_{0.5act}$ as a function of pH gave a pKa of 6.2 ± 0.1 (Figure 1I), while the pKa for E_M of unclamped oocytes expressing CaTOK was 5.8 ± 0.1 (Figure 1M). The pKa value of ∼6 and the rapid onset and reversal of the effects of extracellular acidification suggested an extracellularly exposed imidazole side chain of histidine (pKa ∼6) as the prime candidate for pH sensing in CaTOK channels.

Histidine protonation in the S1-S2 linker forms part of the CaTOK pH sensor

Next, we sought to determine the pH sensitivity of TOK channels cloned from *S. cerevisiae* (ScTOK), *A. fumigatus* (AfTOK), and *C. neoformans* var *neoformans* (CnTOK) (Figure 2A). Interestingly, ScTOK, CnTOK, and AfTOK exhibited limited pH sensitivity, with no pH-dependent change in current density observed across all pH ranges (Figure 2B: upper; Figures S2A–S2F) and almost no pH-dependent shift in the E_M of unclamped oocytes, except for AfTOK, which exhibited a modest −5 mV shift at pH 4.0 (Figure 2C). Sequence alignments revealed a histidine (H144) located in the predicted S1-S2 extracellular linker of CaTOK that was absent from the other TOK channels (Figure 2D). To provide a better insight into the environment of the histidine residue, we used AlphaFold and UCSF Chimera[13–15] to predict and visualize the structure of CaTOK because no high-resolution structure is currently available for any of the TOK channels (Figure S3). The H144 sidechain is predicted to be exposed to the external medium on the extracellular face of the S1-S2 linker of CaTOK (Figure 2E). Its extracellular exposure, absence in the pH-insensitive TOK channels, and a pKa matching that of the pH response-curve for CaTOK (∼6) strongly suggested H144 as the pH sensor. To confirm this, we performed site-directed mutagenesis mutating H144 to either a lysine (H144K), which is constitutively protonated at physiological pH, or to an asparagine (H144N), which is neutral at physiological pH. Baseline analysis of CaTOK-H144K compared to wild type revealed an almost 2-fold increase in current density at +40 mV from 5.6 ± 0. 6 μA to 9.9 ± 1.1 μA. Furthermore, H144K exhibited a −10.2 ± 1.7 mV left shift in the $V_{0.5act}$ at pH 7.5 compared to wild-type CaTOK. The H144N mutation, in contrast, had no effect on either current density or the $V_{0.5act}$ (Figures S4A and S4B). CaTOK-H144K exhibited only modest pH sensitivity compared to wild type, with attenuated increases in outward currents at pH 5.0 and pH 4.0. Additionally, the shift in $V_{0.5act}$ for H144K was reduced by almost half, with a hyperpolarizing shift of −15.7 ± 1.3 mV at pH 5.0 and −16.9 ± 1.4 mV at pH 4.0 (Figures 2F and 2G; Figures S4C–S4E). Similarly, H144N exhibited reduced sensitivity to low extracellular pH compared to wild-type CaTOK, with only minimal increases in current and a −11.1 mV ± 1.3 mV shift in the $V_{0.5act}$ at pH 4.0 (Figures 2H and 2I; Figures S4F–S4H). H144K and H144N mutations each blunted the pH-dependent increase in current at 0 mV, reducing the nearly 3.5-fold increase at pH 5.0 compared to pH 7.5 observed for wild type CaTOK to a <2-fold increase (Figure 2J). Each mutation also attenuated the CaTOK $\Delta V_{0.5act}$ (Figure 2K) and the ΔE_M of unclamped oocytes in response to lowered extracellular pH (Figure 2L). Interestingly, despite significantly blunting CaTOK response to extracellular acidification, mutating H144 failed to completely abolish the effect on current density and $V_{0.5act}$, suggesting that this residue may form only part of a more intricate pH sensing mechanism. To test this hypothesis, we introduced a histidine at the homologous positions in ScTOK, AfTOK, and CnTOK. As expected, introduction of a histidine failed to endow pH sensitivity, with no pH-dependent augmentation in current magnitude or shift in the ΔE_M of unclamped oocytes observed in across pH 7.5–5.0 (Figures S5A–S5D).

Extracellular acidification makes CaTOK more selective for potassium

Previously, we showed that CaTOK is less selective for K^+ over Na^+ than ScTOK, correlating with a more depolarized E_{REV}.[3] In this context, it was notable that the reversal potential of

(E) Mean peak current (measured during prepulse) from traces as in D; *n* = 8–26 per group.
(F) Mean normalized tail current (G/Gmax) for traces as in D; *n* = 8–26 per group.
(G) Averaged traces for CaTOK channels as indicated, expressed in oocytes in the presence of pH 7.5 or pH 8.5. Scale bar upper right; *n* = 9 per group.
(H) Mean normalized tail current (G/Gmax) for traces as in G; *n* = 9 per group.
(I) Averaged traces for CaTOK channel current increase at −20 mV as indicated, in the presence of pH 7.5, pH 5.0, and pH 4.0. Voltage protocol inset; *n* = 8–26 per group.
(J) Exemplar trace showing wash-in pH 5.0 (magenta) and washout pH 7.5 (black) at 0 mV on CaTOK channels expressed in oocytes (*n* = 6).
(K) Mean current increase versus $(pH)^O$ at 0 mV for oocytes expressing CaTOK; *n* = 8–26 per group.
(L) Mean $V_{0.5act}$ versus $(pH)^O$ for oocytes expressing CaTOK; *n* = 8–26 per group.
(M) Mean E_M versus $(pH)^O$ for oocytes expressing CaTOK; *n* = 8–26 per group.

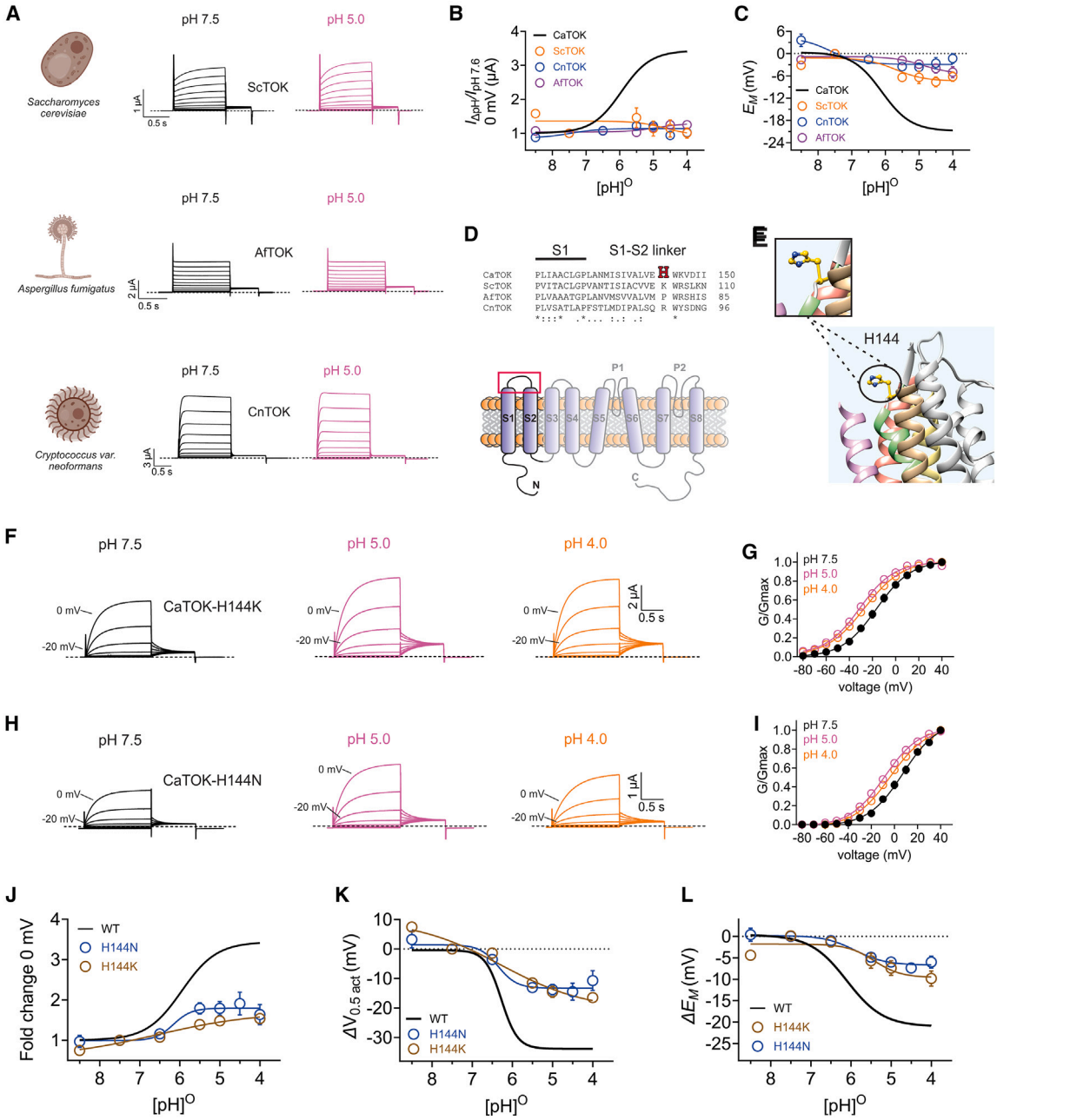

Figure 2. H144 in the CaTOK S1-S2 linker contributes to pH-dependent current augmentation and voltage-dependent activation

Data are represented as mean ± SEM.

(A) Cartoons depicting *Saccharomyces cerevisiae* cell (Top), *Aspergillus fumigatus* (middle), and *Cryptococcus neoformans* (bottom). Averaged traces for ScTOK (Top), AfTOK (Middle), and CnTOK (Bottom) channels as indicated, expressed in oocytes in the presence of pH 7.5 or pH 5.0. Scale bars lower left for each trace; n = 5–11 per group. Created using Biorender.com.

(B) Mean current fold increase versus $(pH)^O$ at 0 mV for ScTOK (magenta), AfTOK (green), and CnTOK (orange), with CaTOK data from Figure 1 for comparison; n = 5–11 per group.

(C) Mean ΔE_M versus $(pH)^O$ for oocytes expressing ScTOK (magenta), AfTOK (green), and CnTOK (orange), with CaTOK data from Figure 1 for comparison; n = 5–11 per group.

(D) Top: Sequence alignment of CaTOK, ScTOK, AfTOK, and CnTOK partial S1 and S1-S2 linker with histidine colored (red). *Residues are identical at this position in all sequences in the alignment; ":", conserved substitutions at this position in all sequences in the alignment; ".", semi-conserved substitutions at this position in all sequences in the alignment. Bottom: Red box highlighting the location of the histidine on the S1-S2 linker of CaTOK channel.

(E) Alpha-Fold predicted structure of CaTOK showing the predicted location of H144 (yellow).

(legend continued on next page)

CaTOK-H144K was more hyperpolarized than for wild-type CaTOK (∼−65 mV, compared to ∼ −40 mV for CaTOK) (Figure 3A). By plotting the reversal potential (E_{REV}) as a function of pH, we found that CaTOK selectivity for K^+ increases as extracellular pH is lowered toward pH 5.0, pushing the E_{REV} closer to E_K, as predicted by the Nernst equation (Figure 3B). Similarly, CaTOK-H144K E_{REV} stays constant at ∼ −65 mV across the pH range, closely mimicking the effect seen for CaTOK at pH 5.0. In contrast, CaTOK-H144N current E_{REV} remains constant at ∼ −40 mV across the pH range, similar to CaTOK at pH 7.5 (Figure 3B). One possible explanation for this observed shift in E_{REV} is that acidic pH is causing conformational changes in the pore, near or at the selectivity filter, altering the ion selectivity of CaTOK. Thus, we conducted pseudo-bi-ionic substitution with monovalent cations to estimate the permeability ratios for CaTOK and CaTOK-H144K at pH 7.5 using a modification of the GHK voltage equation (Equation 2). For wild-type CaTOK, our data replicate our previous findings for all monovalent ions tested (Figure 3C).[3] CaTOK-H144K altered ion selectivity, making the channel more selective for K^+, substantially decreasing relative Na^+, Rb^+, and Cs^+ permeation, explaining the hyperpolarizing shift observed for the E_{REV} (Figure 3C). As CaTOK-H144K mimics the protonated state of a histidine at acidic pH, we next sought to confirm whether a similar effect on ion permeability and E_{REV} was recapitulated by wild-type CaTOK at pH 5.0. Accordingly, switching to pH 5.0 resulted in a hyperpolarizing shift in the E_{REV} of wild-type CaTOK to ∼ −60 mV (Figure 3D) and decreased the permeability of Na^+, Rb^+, and Cs^+, as observed for CaTOK-H144K (Figure 3E).

The second pore domain of CaTOK coordinates a gating mechanism sensitive to extracellular acidification

To investigate the role of the pore domain in CaTOK modulation by extracellular pH, we first generated three chimeras in which we substituted the first pore (P1), second pore (P2), or the C-terminal domains of CaTOK with the equivalent domains of pH insensitive ScTOK (Figures 4A and 4B). Chimera P1 failed to produce discernable currents and therefore could not be studied (data not shown). The C-terminal chimera exhibited reduced current density compared to wild type and failed to produce measurable tail currents (Figures 4C and S6A) but it could be studied to demonstrate that the substitution did not alter sensitivity to pH, with a shift to pH 5.5 increasing currents 5.5-fold at 0 mV (Figures 4C and 4D, upper).

Chimera P2 produced robust outward currents comparable in magnitude to those observed for wild type CaTOK (Figures 4B and S6A). Strikingly, the $V_{0.5act}$ for chimera P2 was −75 mV, representing a −72 mV hyperpolarizing shift compared to wild-type CaTOK (Figure S6B). This substitution significantly weakened the response to extracellular acidification (Fig. 4CD, lower). Subsequent alignments of the P2 domain of CaTOK and ScTOK revealed three clusters containing divergent residues. Using site-directed mutagenesis, residues in CaTOK were substituted with the reciprocal residues in ScTOK, to generate three further chimeric constructs, which we designated P2A-C (Figure 4E). Mutants P2A and P2B exhibited reduced basal current density compared to wild-type CaTOK but had similar $V_{0.5act}$ (Figures 4F, 4G, S6A, S6C, and S6D). Mutant P2C increased basal currents 4-fold and significantly hyperpolarized the $V_{0.5act}$ (−47.9 ± 1.6 mV) (Figures 4F, 4G, S6A, and S6E). Both P2A and P2B exhibited similar pH sensitivity to wild type, with pH 5.5 increasing current density 3.8-fold and 3.5-fold at 0 mV, respectively. Strikingly, mutant P2C almost completely blunted the effect of pH 5.5 on current augmentation, to 1.3-fold at 0 mV, recapitulating the blunted pH effect observed with chimera P2, and effects on $V_{0.5act}$ (Figures 4H and 4I). Interestingly, despite chimera P2 and mutant P2C significantly impairing the effect of acidic pH on current potentiation, neither mutant suppressed the ability of pH 5.5 to hyperpolarize the $V_{0.5act}$, with both mutants displaying similar ∼ −33 mV shifts as seen with wild-type CaTOK (Figures 4I and S6F–S6I).

A crosstalk mechanism between residues H144, V462, and S466 underpins the molecular basis for CaTOK pH sensitivity

Mutant P2C spans a region comprising six amino acids located within the final transmembrane segment (S8) of CaTOK (Figure 5A). To study these residues, all six were mutated individually to the corresponding residues in the pH insensitive ScTOK. All mutants exhibited robust outward current similar in magnitude to that of wild type CaTOK, with the exception of S466I, which was ∼2-fold larger (Figure S7A). Mutants K456R, S458G, and L459A all had a $V_{0.5act}$ akin to that of wild-type CaTOK. Interestingly, V462A and V495L each right-shifted the $V_{0.5act}$, while S466I hyperpolarized the $V_{0.5act}$ by −51mV (Figure S7B). Mutants K456R, S458G, L459A, V462A, and V469L all failed to prevent an increase in CaTOK currents at pH 5.5, with all mutants exhibiting a 3-fold or greater current increase at 0 mV (Figures 5B, 5C, 5E, and S7C). Similarly, the $V_{0.5act}$ of these mutants was shifted ∼ −33 mV at pH 5.5, with the exception of V462, which reduced the hyperpolarizing shift by −11 mV compared to wild type (Figures 5D, 5F, and S7C). Critically, mutant S466I essentially

(F) Averaged traces for CaTOK-H144K channels as indicated, expressed in oocytes in the presence of pH 7.5, pH 5.0, and pH 4.0. Scale bar upper right; n = 6–10 per group.
(G) Mean normalized tail current (G/Gmax) for traces as in F; n = 6–10 per group.
(H) Averaged traces for CaTOK-H144N channels as indicated, expressed in oocytes in the presence of pH 7.5, pH 5.0, and pH 4.0. Scale bar upper right; n = 8–16 per group.
(I) Mean normalized tail current (G/Gmax) for traces as in H; n = 8–16 per group.
(J) Mean current fold increase versus $(pH)^O$ at 0 mV for CaTOK-H144K (orange) and CaTOK-H144N (blue), with CaTOK data from Figure 1 for comparison; n = 6–16 per group.
(K) Mean $\Delta V_{0.5act}$ versus $(pH)^O$ for oocytes expressing for CaTOK-H144K (orange) and CaTOK-H144N (blue), with CaTOK data from Figure 1 for comparison; n = 6–16 per group.
(L) Mean ΔE_M versus $(pH)^O$ for oocytes expressing for CaTOK-H144K (orange) and CaTOK-H144N (blue), with CaTOK data from Figure 1 for comparison; n = 6–16 per group.

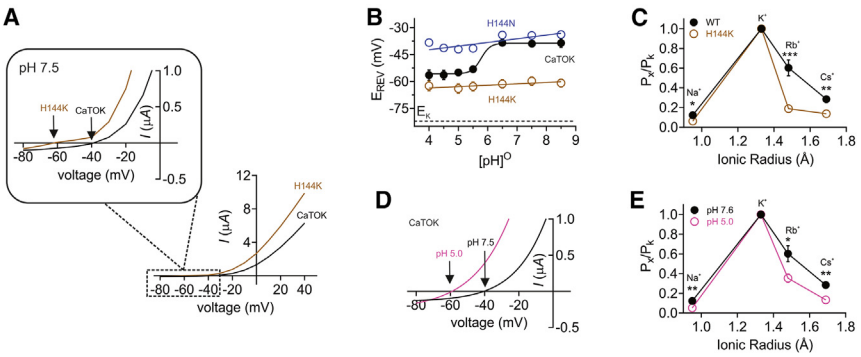

Figure 3. Extracellular protonation increases potassium selectivity via modulation of the pore

Data are represented as mean ± SEM.

(A) Mean peak current (measured during prepulse) for wild type CaTOK (black) and H144K (brown) in the presence of pH 7.5, upper right quadrant shows the reversal potential for each channel as indicated by the arrow; n = 10–26 per group.

(B) Extracellular PH (pH^O) versus reversal potential (E_{REV}) for wild-type and H144 mutant CaTOK channels as indicated, expressed in oocytes. Calculated from traces as in Figure 2; n = 6–26 per group.

(C) Relative ion permeabilities of CaTOK and H144K channels in the presence of pH 7.5 for rubidium (p = 0.0005), sodium (p = 0.0190), and cesium (p = 0.0046); n = 10. Statistical analysis by One-way ANOVA.

(D) Mean peak current (measured during prepulse) for CaTOK in the presence of pH 7.5 (black) and pH 5.0 (pink), the reversal potential of CaTOK in pH 7.5 and pH 5.0 is indicated by the arrow; n = 22–26 per group.

(E) Relative ion permeabilities of CaTOK in the presence of pH 7.5 (black) and pH 5.0 (pink) for rubidium (p = 0.0172), sodium (p = 0.0066), and cesium (p = 0.0014); n = 10. Statistical analysis by One-way ANOVA.

abolished current potentiation in response to pH 5.5, exhibiting only a 25%-fold increase in current at 0 mV (Figures 5B, 5C, 5E, and S7C). Conversely, S466I did not prevent the shift in the $V_{0.5act}$ with pH 5.5 inducing a shift of −31.9 ± 1.6 mV (Figures 5D and 5F). These data reveal that S466 in S8 near the external portion of the pore is integral for facilitating current augmentation in response to extracellular acidification but does not alone perturb the effect of pH on the $V_{0.5act}$.

CaTOK pH modulation is coordinated by H144 in the S1-S2 linker and V462 and S466 in S8

Our data thus far revealed that mutating H144 in the S1-S2 linker reduces current augmentation and $V_{0.5act}$ by extracellular acidification, while mutating S466 in S8 abolishes current augmentation but not the effect of pH on $V_{0.5act}$. Thus, it appears H144 and S466 (Figure 6A) are working in tandem to contribute to the different effects elicited by acidic pH. To validate this prediction, we generated a double mutant, CaTOK-H144N,S466I (Figures S8A and S8B), and found that this modification substantially reduced the effect of pH 5.5 on current augmentation, such that maximal peak current increase at 0 mV was reduced from 3-fold to being barely distinguishable from control (Figures 6B and 6C, Figures S8C and S8D). The effect of pH 5.5 on the $V_{0.5act}$ of CaTOK-H144N,S466I was almost identical to its effect on CaTOK-H144N, reducing the hyperpolarizing shift by −18.4 mV, to −14.7 ± 1.5 mV compared to −33 mV for wild-type CaTOK (Figure 6D; Figure S8E); this pattern was recapitulated in effects on E_M of unclamped oocytes (Figure 6E). However, this meant that as for CaTOK-H144N, CaTOK-H144N,S466I still exhibited a hyperpolarizing shift in $V_{0.5act}$ in response to acidic pH, suggesting contribution from another residue. Earlier, we observed that V462A reduced the effect of pH 5.5 on the $V_{0.5act}$ by 11 mV, raising the possibility that this residue could also form part of the pH-responsive elements. Thus, we generated and characterized a triple mutant channel, Ca-TOK-H144N,S466I,V462A (Ca-TOK-x3, Figures S8A and S8B). Strongly supporting that all three residues constitute the pH-responsive element, the triple-mutant channel exhibited negligible low pH-induced current augmentation at 0 mV similar to CaTOK-H144N,S466I (Figures 6C and 6F; Figures S8F and S8G) and less than half the low pH-induced hyperpolarization of $V_{0.5act}$ observed for CaTOK-H144N,S466I (Figures 6D and 6G; Figure S8H) with a negligible low pH-induced hyperpolarization of the E_M (Figure 6E).

Coexpression of CaTOK wild-type and CaTOK-H144N,S466I,V462A reveals that both subunits are required for pH sensing

We next investigated whether both subunits of the CaTOK homodimer are required for pH sensitivity by coexpressing CaTOK wild type and CaTOK-H144N,S466I,V462A (Figure 7A). Interestingly, the effect of pH 5.0 and pH 4.0 was negligible, with no significant increases in current density observed across all voltage ranges (Figures 7B–7E). Acidic pH also had no effect on the $V_{0.5act}$ of channels formed after equal co-expression of wild type and CaTOK-H144N,S466I,V462A, reducing the hyperpolarizing shift by −31.8 mV, to −1.4 ± 0.8 at pH 5.0 and −28.4 mV, to −4.8 ± 0.7 at pH 4.0, almost identical to the reduction in voltage-dependent activation observed for CaTOK-H144N,S466I,V462A (Figures 7E and 7F). Similarly, no effect of acidic pH was observed on E_M of unclamped oocytes (Figure 7G). In Figure 3 we revealed that acidic pH shifted the reversal potential of wild-type CaTOK closer to E_K by altering ion selectivity, making CaTOK more selective for K^+, an effect we hypothesize is due to a pH-dependent conformational change at the selectivity filter (Figures 3D and 3E). Thus, we wanted to investigate whether pH-dependent changes in ion selectivity still occur in channels formed by equal co-expression of wild type and CaTOK-H144N,S466I,V462A. Strikingly, the effect of acidic pH on the reversal potential was negligible (−54 mV at pH 7.5, compared to −55 mV at pH 5.0) compared to the ∼-20 mV shift observed for wild-type CaTOK at the same pH range, suggesting pH no longer effects ion selectivity (Figure 7H).

To confirm our suspicions, we conducted pseudo-bi-ionic substitution experiments. As expected, switching to pH 5.0 had no effect on the permeability of Na^+, Rb^+, and Cs^+,

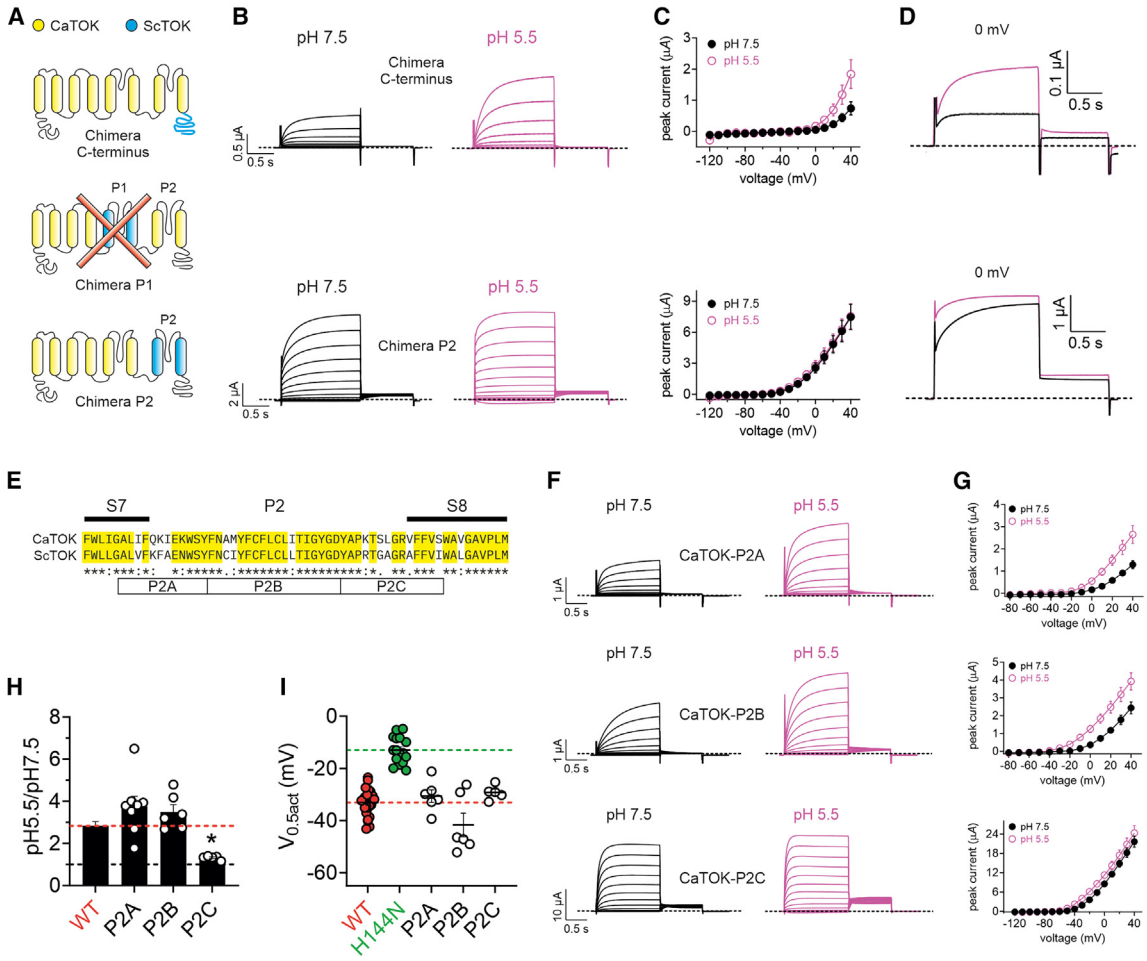

Figure 4. Residues in CaTOK S8 are required for current augmentation, but not hyperpolarization of $V_{0.5act}$, by acidic pH

Data are represented as mean ± SEM.

(A) Cartoons depicting the topology of CaTOK (yellow) and ScTOK (blue) chimeras. Top: C-terminal chimera; Bottom: P2 chimera. Averaged traces for CaTOK-ScTOK chimeric channels as indicated, expressed in oocytes in the presence of pH 7.5 and pH 5.5. Scale bar lower left; n = 8–10 per group.

(B) Mean peak current (measured during prepulse) from traces as in A; n = 8–10 per group.

(C) Mean ΔE_M of unclamped oocytes as in A; n = 8–10 per group.

(D) Averaged traces at 0 mV as indicated, expressed in oocytes in the presence of pH 7.5 and pH 5.5; n = 8–10 per group.

(E) Sequence alignment of CaTOK versus ScTOK S7-P2-S8 region. Boxes P2A, P2B, and P2C indicate clusters of divergent sequences. *Residues are identical at this position in all sequences in the alignment; ":", conserved substitutions at this position in all sequences in the alignment; ".", semi-conserved substitutions at this position in all sequences in the alignment.

(F) Averaged traces for P2A, P2B, and P2C mutant channels as indicated, expressed in oocytes in the presence of pH 7.5 and pH 5.5. Scale bar lower left; n = 5–8 per group.

(G) Mean peak current (measured during prepulse) from traces as in F; n = 5–8 per group.

(H) Fold increase at 0 mV as in G. Black dashed line indicates no change; Red dashed line indicates current-fold increase for wild type CaTOK; n = 5–26 per group. Statistical significance for relative current for P2C was $^*p$ = 0.0156 by One-way ANOVA.

(I) Mean $\Delta V_{0.5act}$ for wild-type and mutant CaTOK channels. Green dashed line indicates the mean $\Delta V_{0.5act}$ for CaTOK-H144N; Red dashed line indicates mean $\Delta V_{0.5act}$ for wild-type CaTOK; n = 5–26 per group.

explaining the reduced hyperpolarizing shift observed for the E_{REV} (Figure 7I). This is in stark contrast to wild-type CaTOK, which exhibited markedly decreased permeability of Na^+, Rb^+, and Cs^+ at pH 5.0 (Figure 7J). Assuming a binomial distribution of dimeric CaTOK channel types formed by equal co-expression of wild type and mutant CaTOK, one would expect ¼ channels to be wild type, ¼ homomeric mutant, and ½ heteromeric wild-type/mutant. The most likely explanation from the data are therefore that heteromeric wild-type/mutant CaTOK channels behave similarly to homomeric mutant channels, i.e., are pH-insensitive, and only a small fraction of the channels (the homomeric wild-type channels) are pH-sensitive. Thus, the pH sensor of CaTOK requires all of the pH-sensing amino acids on both of the subunits within the homodimer to confer pH sensitivity.

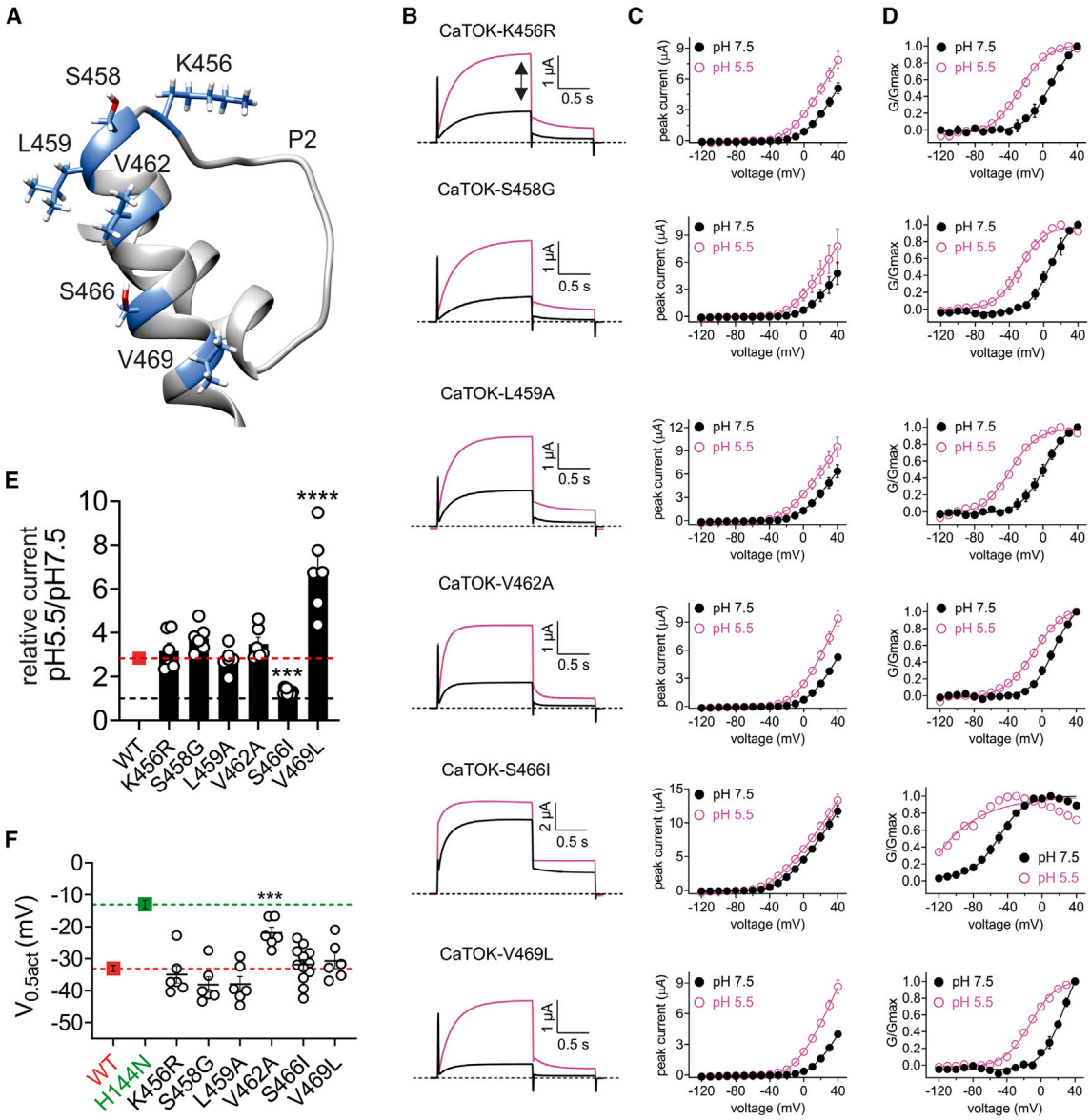

Figure 5. S466 is the molecular determinant for current augmentation, but not hyperpolarization of $V_{0.5act}$, by acidic pH

Data are represented as mean ± SEM.

(A) Alpha-Fold predicted structure of P2 and the extracellular end of S8 of CaTOK showing the predicted locations of the six residues within the P2C region (cornflower blue).

(B) Averaged traces for S8 mutant currents at 0 mV as indicated, in the presence of pH 7.5 and pH 5.5. Black dashed line indicates no change; Red dashed line indicates current-fold increase for wild type CaTOK; n = 6–11 per group.

(C) Mean peak current (measured during prepulse) from traces as in B; n = 6–11 per group.

(D) Mean normalized tail current (G/Gmax) for traces as in B; n = 6–12 per group.

(E) Fold increase at 0 mV as in G. Black dashed line indicates no change; Red dashed line indicates current-fold increase for wild type CaTOK; n = 6–12 per group. Statistical significance for comparison of relative current for S466I was ***p = 0.0002 and V496L was ****<0.0001 by One-way ANOVA.

(F) Mean $\Delta V_{0.5act}$ for wild-type and mutant CaTOK channels. Green dashed line indicates the mean $\Delta V_{0.5act}$ for CaTOK-H144N; Red dashed line indicates mean $\Delta V_{0.5act}$ for wild-type CaTOK; n = 6–12 per group. Statistical significance for comparison of $\Delta V_{0.5act}$ for V462A was ***p = 0.0001 by One-way ANOVA.

DISCUSSION

C. albicans is unusual among fungal pathogens in its ability to colonize in a broad range of external pH, surviving in both extremely acidic (pH $\leq$ 2) and extremely alkaline (pH $\geq$ 10) conditions. This is due in part to *C. albicans* having a malleable cytosolic pH, which can range between pH 5.8 and pH 9.0 compared to non-pathogenic yeast species such as *S. cerevisiae*, which maintain a cytosolic pH between 6.0 and 7.0.[16] In fact, significant alkalinization of the cytosol precedes hyphal formation in

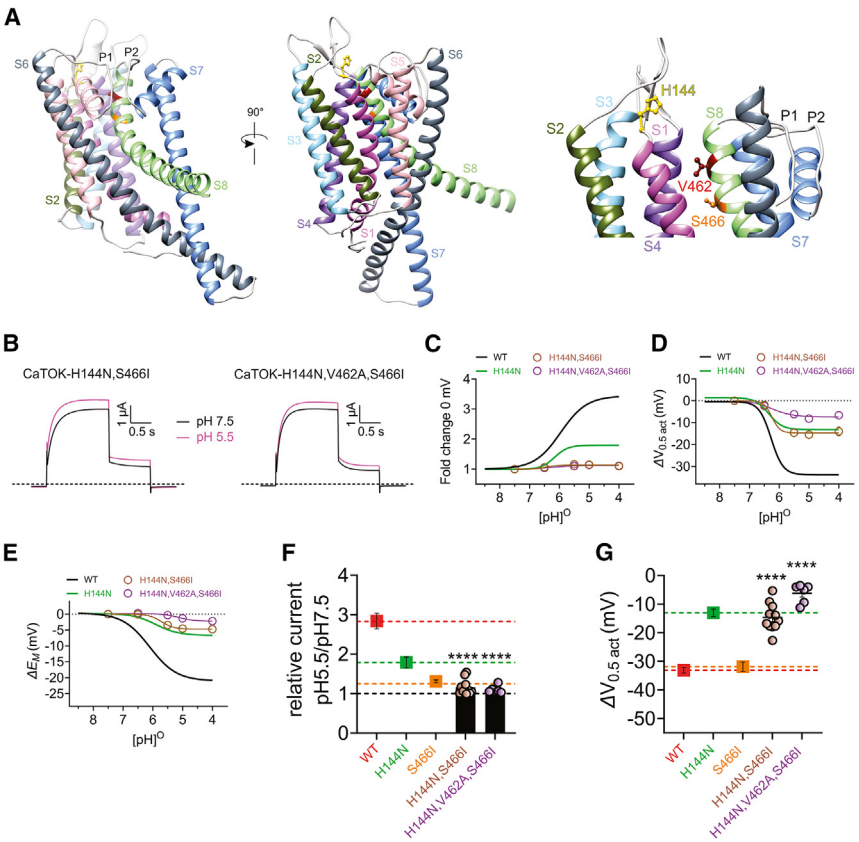

Figure 6. Residues H144, V462, and S446 participate cooperatively to sense and mechanically transduce CaTOK responses to pH

Data are represented as mean ± SEM.

(A) Alpha-Fold predicted structure showing the proximity of H144 (yellow) in the S1-S2 linker to V462 (red) and S466 (orange) in the extracellular end of CaTOK S8.

(B) Averaged traces for H144N-S466I (left) and H144N,V462A,S446I (right) mutant CaTOK currents at 0 mV as indicated, in the presence of pH 7.5 and pH 5.5; n = 5–11 per group.

(C) Mean current fold increase versus $(pH)^O$ at 0 mV for H144N-S466I (brown) and H144N,V462A,S466I (purple), with CaTOK data from Figure 1 and H144N data from Figure 2 for comparison; n = 5–11 per group.

(D) Mean $\Delta V_{0.5act}$ versus $(pH)^O$ for H144N,S466I (brown) and H144N,V462A,S466I (purple), with CaTOK data from Figure 1 and H144N data from Figure 2 for comparison; n = 5–11 per group.

(E) Mean ΔE_M versus $(pH)^O$ for H144N,S466I (brown) and H144N,V462A,S466I (purple), with CaTOK data from Figure 1 and H144N data from Figure 2 for comparison; n = 5–11 per group.

(F) Fold increase at 0 mV as in C for H144N,S466I (brown) and H144N,V462A,S466I (purple), with CaTOK (red dashed line), H144N (green dashed line), and S466I (orange dashed line) for comparison. Black dashed line reflects no change; n = 5–11 per group. Statistical significance for comparison of relative current for H144N, S466I was ****<0.0001 and H144N, V462A, S466I was ****<0.0001 by One-way ANOVA.

(G) Mean $\Delta V_{0.5act}$ as in D for H144N,S466I (brown) and H144N,V462A,S466I (purple), with CaTOK (red dashed line), H144N (green dashed line), and S466I (orange dashed line) for comparison. Black dashed line reflects no change; n = 5–11 per group. Statistical significance for comparison of $\Delta V_{0.5act}$ for H144N, S466I was ****<0.0001 and H144N, V462A, S466I was ****<0.0001 by One-way ANOVA.

C. albicans, with an internal pH of 7.0 initiating the outgrowth of germ tubes.[17] It is thought that Pma1p, a plasma membrane H^+-ATPase, mediates this process and is also a major driver in setting yeast membrane potential via H^+ movement across the membrane.[18] This pH gradient drives nutrient uptake via secondary transporters, including K^+ uptake, which can reach 200–300 mM inside the yeast cell. In the absence of energy supply, where Pma1p is no longer helping to dictate the membrane potential, or in the presence of some other stressor, yeast cells will depolarize.

Several studies have implicated TOK channels in critical processes such as K^+ homeostasis, membrane potential regulation, and osmoregulation.[19,20] Rather than setting membrane potential *per se* (as do analogous K^+ channels in higher animals), TOK channels are thought to mitigate the negative impact of yeast cell depolarization, i.e., play a gatekeeper role in maintaining membrane potential under stress. When membrane potential shifts positive to E_K, TOK channels become active and stabilize the membrane potential, preventing further excessive depolarization which would likely result in cell death. They do not switch on at a set voltage (as do voltage gated K^+ channels) but rather at the membrane potential determined by E_K under the specific conditions the cell is experiencing. Therefore, while some studies have shown *Candida* resting membrane potential to be as hyperpolarized as, e.g., −120 mV, with internal K^+ at 200–300 mM, external K^+ at around 4 mM (body fluid) and at a host mammalian body temp of 37°C, the Nernst equation predicts TOK activation at around −100 to −115 mV, which would be in the protective range for the microbe under those conditions. The shifting voltage dependence of TOK activation permits the yeast to adapt to different environmental K^+ conditions or fluctuations in internal K^+. The proposed model for TOK channels' capacity to only pass current positive to E_K (thus ensuring they are outward rectifiers despite lacking a traditional voltage sensing apparatus) is that the K^+ reversal potential determines ion occupancy and therefore conductivity of a selectivity filter that can sample both intracellular and extracellular ion concentrations and thus acts as the channel gate (similar two mammalian K2P channels; see in the further text).[3]

Prasad and Hofer measured resting membrane potential (E_M) for *C. albicans* at a range of external pH values and found it to be between −72 and −78 mV at pH 4.5–5.5, hyperpolarizing to −100 mV at pH 7.5 and >−120 mV at pH 8.5.[21] In their study, E_M was measured indirectly from the distribution of tetraphenylphosphonium ions, which may even overestimate E_M compared to when quantified by direct microelectrode measurement (i.e., the actual values may be less negative).[22] At pH 4.0–5.5 we observed a substantial negative shift in the voltage dependence

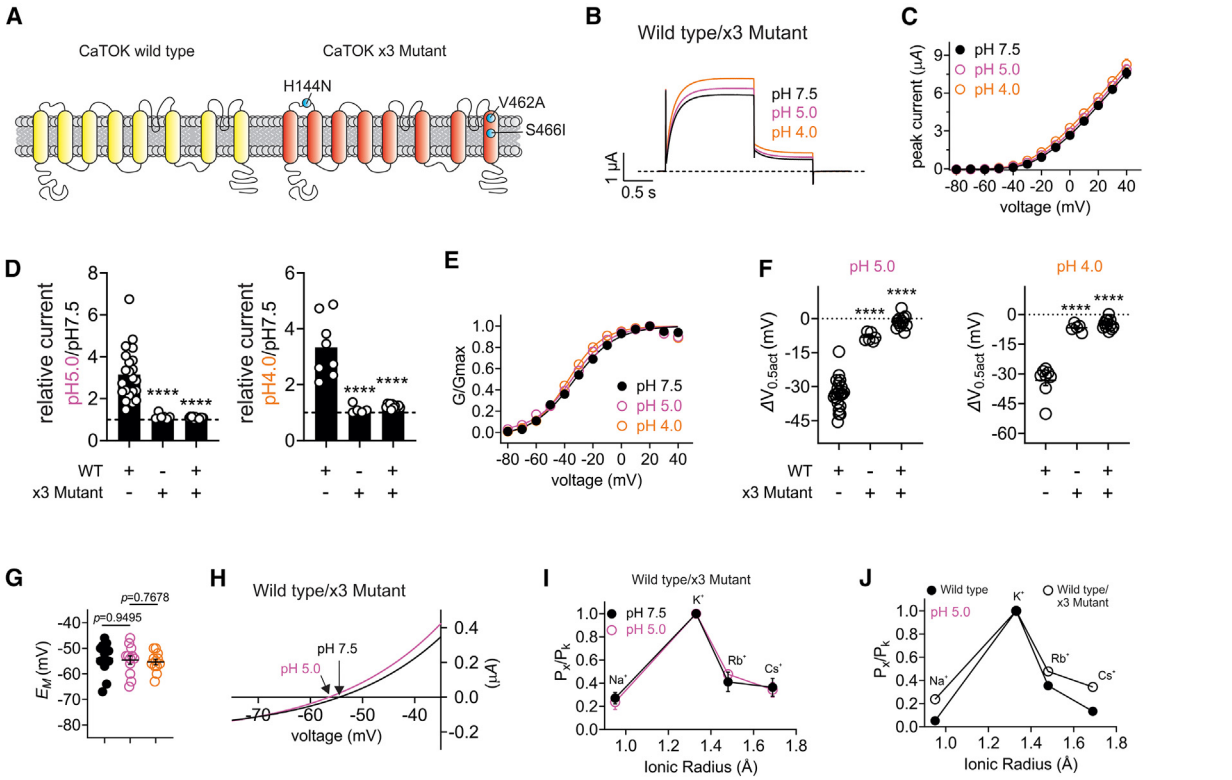

Figure 7. CaTOK requires both subunits to confer pH sensitivity

Data are represented as mean ± SEM.

(A) Schematic of CaTOK wild type (yellow) and H144N,V462A,S446I mutant (red).

(B) Averaged traces for CaTOK wild type/x3 mutant currents at 0 mV as indicated, in the presence of pH 7.5, pH 5.0, pH 4.0: n = 12 per group.

(C) Mean peak current (measured during prepulse) from traces as in B; n = 12 per group.

(D) Fold increase at 0 mV as in C for CaTOK wild type, ×3 mutant (H144N,V462A,S466I), and wild type/x3 mutant heterodimer in the presence of pH 5.0 (left) and pH 4.0 (right). Black dashed line reflects no change; n = 8–22 per group. Statistical significance for comparison of relative current for ×3 mutant (H144N,V462A,S466I) was ****<0.0001 and wild type/x3 mutant heterodimer was ****<0.0001 at pH 5.0 and ×3 mutant (H144N,V462A,S466I) was ****<0.0001 and wild type/x3 mutant heterodimer was ****<0.0001 at pH 4.0 by One-way ANOVA..

(E) Mean normalized tail current (G/Gmax) for traces as in B; n = 12 per group.

(F) Mean $\Delta V_{0.5act}$ as in E for CaTOK wild type, ×3 mutant (H144N,V462A,S466I), and wild type/x3 mutant heterodimer in the presence of pH 5.0 (left) and pH 4.0 (right). Black dashed line reflects no change; n = 8–22 per group. Statistical significance for comparison of $\Delta V_{0.5act}$ for ×3 mutant (H144N,V462A,S466I) was ****<0.0001 and wild type/x3 mutant heterodimer was ****<0.0001 at pH 5.0 and ×3 mutant (H144N,V462A,S466I) was ****<0.0001 and wild type/x3 mutant heterodimer was ****<0.0001 at pH 4.0 by One-way ANOVA..

(G) Mean E_M versus $(pH)^O$ as in B; n = 12 per group. Statistical analysis was by One-way ANOVA.

(H) Mean peak current (measured during prepulse) for wild type/x3 mutant heterodimers in the presence of pH 7.5 (black) and pH 5.0 (pink) as in C showing the reversal potential for as indicated by the arrow; n = 12 per group.

(I) Relative ion permeabilities of wild type/x3 mutant heterodimers in the presence of pH 7.5 (black) and pH 5.0 (pink); n = 5–8.

(J) Relative ion permeabilities of wild-type CaTOK (black circles) and wild type/x3 mutant heterodimers (open circles) in the presence of pH 5.0; n = 8–10.

of CaTOK activation and overall current augmentation such that it was open even as far negative at −80 mV (Figure 1F). Thus, the low pH-induced shift in voltage dependence of CaTOK activation coincides with a low pH-induced shift in *C. albicans* E_M, which would be predicted to endow CaTOK with a greater capacity to protect against depolarization of *C. albicans* E_M under acidic extracellular conditions.

A particularly striking finding of our present study was that only CaTOK was pH sensitive among the TOK channels tested. Despite belonging to the same family, the homology between the channels is relatively low, with ScTOK at 36% showing the closest homology to CaTOK. One possible explanation could lie with the route of infection of the host organism. *C. albicans* is uniquely tuned to its environment, using changes in temperature, high CO_2, nutrient deprivation, and pH to initiate its transition from a commensal round yeast into a virulent filamentous hyphal form.[23–26] This is, particularly advantageous for *C. albicans* when it colonizes within the commensal flora of the oral, genital, and intestinal mucosa,[27] where these parameters fluctuate regularly. The primary reservoir of *C. albicans* is in the gastrointestinal (GI) tract, which has perhaps the most dynamic range of pH (<2.0 to >10.0), from highly acidic in the stomach to neutral or alkaline in other parts of the gut.[28] This is in stark contrast to *A. fumigatus* and *C. neoformans*, which do not infect

via these routes but rather attach to airway epithelia or within the pulmonary alveoli which are subject to less dynamic changes in pH. Thus, it could be speculated that CaTOK pH sensitivity arises from an evolutionary advantage for *C. albicans* to be responsive to pH changes, while the insensitivity of AfTOK and CnTOK results from a lack of evolutionary pressure on *A. fumigatus* and *C. neoformans* to be responsive to pH.

Differential modulation by pH is not, however, exclusive to TOK channels, even among channels with two P domains. TASK1 and TASK3 were named for their acid-sensitivity, whereby protonation of a His in the first pore domain inhibits the channel across the physiologic pH range.[29–31] TREK-1 and TREK-2 are regulated by a range of stimuli, including mechanical stretch, osmolarity, heat, polyunsaturated fatty acids, and pH.[32–36] TREK channel responses to pH are contrasting, with TREK-1 robustly inhibited by acidic pH, while TREK-2 is activated by external acidification, differences attributed to the electrostatic interactions between the conserved histidine and their neighboring residues in the distal end of the P2 domain.[37] The mechanism of TREK-1 inhibition by external pH is governed by two histidine residues (H87 and H141) in the external S1-S2 linker of the channel. Protonation of these histidine residues is thought to facilitate the collapse of the selectivity filter region, which acts as the TREK-1 channel gate, through hydrogen bond formation with a proximal glutamate (E84).[38] However, the inhibitory effect of acidic pH on TREK-1 currents is diminished significantly by gain-of-function (GOF) mutations to residues lining the pore, suggesting that these GOF mutations act by uncoupling the sensory and gating apparatus of TREK-1.[39]

The AlphaFold-generated structure prediction for CaTOK shows H144 in close proximity to V462 and S466; however, how these residues interact in order to confer pH sensitivity remains to be elucidated. In TREK-1 and TREK-2, a histidine in the first pore loop is thought to interact with charged residues in the second pore to confer inhibition and activation, respectively.[37] It was proposed that negatively charged residues in the P2 domain of TREK-1 attract the protonated imidazole side chain of the histidine and induce a conformational change more likely to favor the closed-state. Whereas in TREK-2, the same region is comprised of basic residues and likely repels the protonated histidine, resulting in the opposite effect.[37] There is no charge difference in the region P2C domain of CaTOK and pH insensitive ScTOK, suggesting the electrostatic mechanism model of pH gating for TREK channels does not apply here.

The role of TOK channels in fungal physiology is currently incompletely understood. Deletion or overexpression of TOK1 in *S. cerevisiae* has been shown to depolarize and hyperpolarize the membrane potential, respectively,[19] as well providing the molecular basis for both killer toxin activity and immunity.[9,10] Conversely, TOK1 inhibition has been proposed as integral in protecting yeast during hyperosmotic stress, whereby phosphorylation of the mitogen-activated protein kinase Hog1P inhibits TOK1 channel activity leading to membrane depolarization and reduced secondary ion flow into the cell.[40] Our study identifies CaTOK as a potential molecular sensor for *C. albicans* pH sensitivity that may contribute to pH-dependent hyphal formation, a key virulence trait, and therefore highlights CaTOK as a potential therapeutic target.

Limitations of the study

This study was performed *in vitro* using cellular electrophysiology of currents from TOK channels heterologously expressed in *Xenopus* oocytes; future studies could examine TOK function in the context of *Candida* itself. In addition, we rely on AlphaFold-predicted TOK channel structures in the absence of high-resolution experimental data of the TOK channel structure.

RESOURCE AVAILABILITY

Lead contact

Further information and requests for resources and reagents should be directed to and will be fulfilled by the lead contact, Dr. Geoffrey W. Abbott (abbottg@hs.uci.edu).

Materials availability

This study did not generate new unique reagents; channel constructs are available upon request.

Data and code availability

- Electrophysiology source data have been deposited at Dryad and are publicly available as of the date of publication: Accession numbers are listed in the key resources table.
- There are no applicable codes.
- There are no other applicable items.

ACKNOWLEDGMENTS

This study was supported by the National Institutes of Health, National Institute of General Medical Sciences (GM130377) to G.W.A., The Royal Society (RGS\R1\201026) to RWM and Biotechnology and Biological Sciences Research Council (BBSRC), UK, grant number BB/J006114/1 to A.L.

AUTHOR CONTRIBUTIONS

R.W.M., G.W.A., S.A.N.G., and A.L. conceived the study; A.L. and Z.A.M. generated and performed initial characterization of some constructs; R.W.M. and C.L.I. conducted TEVC studies and analyzed data; R.W.M., G.W.A., S.A.N.G., and A.L. oversaw and/or obtained funding for the project; R.W.M. prepared the figures, R.W.M. and G.W.A. wrote the manuscript; all authors contributed to editing the manuscript.

DECLARATION OF INTERESTS

The authors declare no competing interests.

STAR★METHODS

Detailed methods are provided in the online version of this paper and include the following:

- KEY RESOURCES TABLE
- EXPERIMENTAL MODEL DETAILS
- METHOD DETAILS
  - Channel subunit cRNA preparation and Xenopus laevis oocyte injection
  - Two-electrode voltage clamp (TEVC)
  - Relative permeability calculations
  - CaTOK structure prediction
- QUANTIFICATION AND STATISTICAL ANALYSIS

SUPPLEMENTAL INFORMATION

Supplemental information can be found online at https://doi.org/10.1016/j.isci.2024.111451.

Received: June 18, 2024
Revised: September 18, 2024
Accepted: November 19, 2024
Published: November 22, 2024

REFERENCES

1. Ketchum, K.A., Joiner, W.J., Sellers, A.J., Kaczmarek, L.K., and Goldstein, S.A. (1995). A new family of outwardly rectifying potassium channel proteins with two pore domains in tandem. Nature *376*, 690–695.
2. Roberts, S.K. (2003). TOK homologue in Neurospora crassa: first cloning and functional characterization of an ion channel in a filamentous fungus. Eukaryot. Cell *2*, 181–190.
3. Lewis, A., McCrossan, Z.A., Manville, R.W., Popa, M.O., Cuello, L.G., and Goldstein, S.A.N. (2020). TOK channels use the two gates in classical K(+) channels to achieve outward rectification. Faseb. J. *34*, 8902–8919.
4. Denning, D.W. (2024). Global incidence and mortality of severe fungal disease. Lancet Infect. Dis. *24*, e428–e438. https://doi.org/10.1016/s1473-3099(23)00692-8.
5. AndréS, M.T., Viejo-DíAz, M., and Fierro, J.F. (2008). Human Lactoferrin Induces Apoptosis-Like Cell Death inCandida albicans: Critical Role of K+-Channel-Mediated K+Efflux. Antimicrob. Agents Chemother. *52*, 4081–4088. https://doi.org/10.1128/aac.01597-07.
6. Baev, D., Rivetta, A., Li, X.S., Vylkova, S., Bashi, E., Slayman, C.L., and Edgerton, M. (2003). Killing of Candida albicans by Human Salivary Histatin 5 Is Modulated, but Not Determined, by the Potassium Channel TOK1. Infect. Immun. *71*, 3251–3260. https://doi.org/10.1128/iai.71.6.3251-3260.2003.
7. Lee, W., and Lee, D.G. (2018). Potential role of potassium and chloride channels in regulation of silymarin-induced apoptosis in Candida albicans. IUBMB Life *70*, 197–206. https://doi.org/10.1002/iub.1716.
8. Yun, J., and Lee, D.G. (2017). Role of potassium channels in chlorogenic acid-induced apoptotic volume decrease and cell cycle arrest in Candida albicans. Biochim. Biophys. Acta Gen. Subj. *1861*, 585–592. https://doi.org/10.1016/j.bbagen.2016.12.026.
9. Ahmed, A., Sesti, F., Ilan, N., Shih, T.M., Sturley, S.L., and Goldstein, S.A. (1999). A molecular target for viral killer toxin. Cell *99*, 283–291. https://doi.org/10.1016/s0092-8674(00)81659-1.
10. Sesti, F., Shih, T.M., Nikolaeva, N., and Goldstein, S.A. (2001). Immunity to K1 killer toxin: internal TOK1 blockade. Cell *105*, 637–644.
11. Lesage, F., Guillemare, E., Fink, M., Duprat, F., Lazdunski, M., Romey, G., and Barhanin, J. (1996). A pH-sensitive Yeast Outward Rectifier K+ Channel with Two Pore Domains and Novel Gating Properties. J. Biol. Chem. *271*, 4183–4187. https://doi.org/10.1074/jbc.271.8.4183.
12. Bertl, A., Bihler, H., Reid, J.D., Kettner, C., and Slayman, C.L. (1998). Physiological characterization of the yeast plasma membrane outward rectifying K + channel, DUK1 (TOK1), in situ. J. Membr. Biol. *162*, 67–80. https://doi.org/10.1007/s002329900343.
13. Jumper, J., Evans, R., Pritzel, A., Green, T., Figurnov, M., Ronneberger, O., Tunyasuvunakool, K., Bates, R., Žídek, A., Potapenko, A., et al. (2021). Highly accurate protein structure prediction with AlphaFold. Nature *596*, 583–589. https://doi.org/10.1038/s41586-021-03819-2.
14. Varadi, M., Anyango, S., Deshpande, M., Nair, S., Natassia, C., Yordanova, G., Yuan, D., Stroe, O., Wood, G., Laydon, A., et al. (2022). AlphaFold Protein Structure Database: massively expanding the structural coverage of protein-sequence space with high-accuracy models. Nucleic Acids Res. *50*, D439–D444. https://doi.org/10.1093/nar/gkab1061.
15. Pettersen, E.F., Goddard, T.D., Huang, C.C., Couch, G.S., Greenblatt, D.M., Meng, E.C., and Ferrin, T.E. (2004). UCSF Chimera–a visualization system for exploratory research and analysis. J. Comput. Chem. *25*, 1605–1612. https://doi.org/10.1002/jcc.20084.
16. Rane, H.S., Hayek, S.R., Frye, J.E., Abeyta, E.L., Bernardo, S.M., Parra, K.J., and Lee, S.A. (2019). Candida albicans Pma1p Contributes to Growth, pH Homeostasis, and Hyphal Formation. Front. Microbiol. *10*, 1012.
17. Stewart, E., Gow, N.A., and Bowen, D.V. (1988). Cytoplasmic alkalinization during germ tube formation in Candida albicans. J. Gen. Microbiol. *134*, 1079–1087.
18. Goossens, A., De La Fuente, N., Forment, J., Serrano, R., and Portillo, F. (2000). Regulation of yeast H+-ATPASe by protein kinases belonging to a family dedicated to activation of plasma membrane transporters. Mol. Cell Biol. *20*, 7654–7661. https://doi.org/10.1128/mcb.20.20.7654-7661.2000.
19. Maresova, L., Urbankova, E., Gaskova, D., and Sychrova, H. (2006). Measurements of plasma membrane potential changes in Saccharomyces cerevisiae cells reveal the importance of the Tok1 channel in membrane potential maintenance. FEMS Yeast Res. *6*, 1039–1046.
20. Zahumenský, J., Jančíková, I., Drietomská, A., Švenkrtová, A., Hlaváček, O., Hendrych, T., Plášek, J., Sigler, K., and Gášková, D. (2017). Yeast Tok1p channel is a major contributor to membrane potential maintenance under chemical stress. Biochim. Biophys. Acta Biomembr. *1859*, 1974–1985. https://doi.org/10.1016/j.bbamem.2017.06.019.
21. Prasad, R., and Höfer, M. (1986). Tetraphenylphosphonium is an indicator of negative membrane potential in Candida albicans. Biochim. Biophys. Acta Biomembr. *861*, 377–380. https://doi.org/10.1016/0005-2736(86)90442-6.
22. Vacata, V., Kotyk, A., and Sigler, K. (1981). Membrane potential in yeast cells measured by direct and indirect methods. Biochim. Biophys. Acta *643*, 265–268. https://doi.org/10.1016/0005-2736(81)90241-8.
23. Shapiro, R.S., Robbins, N., and Cowen, L.E. (2011). Regulatory circuitry governing fungal development, drug resistance, and disease. Microbiol. Mol. Biol. Rev. *75*, 213–267. https://doi.org/10.1128/mmbr.00045-10.
24. Klengel, T., Liang, W.J., Chaloupka, J., Ruoff, C., Schröppel, K., Naglik, J.R., Eckert, S.E., Mogensen, E.G., Haynes, K., Tuite, M.F., et al. (2005). Fungal adenylyl cyclase integrates CO2 sensing with cAMP signaling and virulence. Curr. Biol. *15*, 2021–2026C.
25. Schrevens, S., Van Zeebroeck, G., Riedelberger, M., Tournu, H., Kuchler, K., and Van Dijck, P. (2018). Methionine is required for cAMP-PKA-mediated morphogenesis and virulence of Candida albicans. Mol. Microbiol. *108*, 258–275. https://doi.org/10.1111/mmi.13933.
26. Lo, H.J., Köhler, J.R., DiDomenico, B., Loebenberg, D., Cacciapuoti, A., and Fink, G.R. (1997). Nonfilamentous C. albicans Mutants Are Avirulent. Cell *90*, 939–949. https://doi.org/10.1016/s0092-8674(00)80358-x.
27. Gow, N.A.R., van de Veerdonk, F.L., Brown, A.J.P., and Netea, M.G. (2011). Candida albicans morphogenesis and host defence: discriminating invasion from colonization. Nat. Rev. Microbiol. *10*, 112–122.
28. Biswas, S., Van Dijck, P., and Datta, A. (2007). Environmental sensing and signal transduction pathways regulating morphopathogenic determinants of Candida albicans. Microbiol. Mol. Biol. Rev. *71*, 348–376.
29. Lopes, C.M., Gallagher, P.G., Buck, M.E., Butler, M.H., and Goldstein, S.A. (2000). Proton block and voltage gating are potassium-dependent in the cardiac leak channel KCNK3. J. Biol. Chem. *275*, 16969–16978. https://doi.org/10.1074/jbc.m001948200.
30. Lopes, C.M., Zilberberg, N., and Goldstein, S.A. (2001). Block of KCNK3 by protons. Evidence that 2-P-domain potassium channel subunits function as homodimers. J. Biol. Chem. *276*, 24449–24452. https://doi.org/10.1074/jbc.c100184200.
31. Ma, L., Zhang, X., Zhou, M., and Chen, H. (2012). Acid-sensitive TWIK and TASK Two-pore Domain Potassium Channels Change Ion Selectivity and Become Permeable to Sodium in Extracellular Acidification. J. Biol. Chem. *287*, 37145–37153. https://doi.org/10.1074/jbc.m112.398164.
32. Patel, A.J., Honoré, E., Maingret, F., Lesage, F., Fink, M., Duprat, F., and Lazdunski, M. (1998). A mammalian two pore domain mechano-gated S-like K+ channel. EMBO J. *17*, 4283–4290. https://doi.org/10.1093/emboj/17.15.4283.

33. Maingret, F., Patel, A.J., Lesage, F., Lazdunski, M., and Honoré, E. (1999). Mechano- or acid stimulation, two interactive modes of activation of the TREK-1 potassium channel. J. Biol. Chem. *274*, 26691–26696. https://doi.org/10.1074/jbc.274.38.26691.

34. Kim, Y., Gnatenco, C., Bang, H., and Kim, D. (2001). Localization of TREK-2 K + channel domains that regulate channel kinetics and sensitivity to pressure, fatty acids and pH i. Pflügers Archiv *442*, 952–960. https://doi.org/10.1007/s004240100626.

35. Maingret, F., Lauritzen, I., Patel, A.J., Heurteaux, C., Reyes, R., Lesage, F., Lazdunski, M., and Honoré, E. (2000). TREK-1 is a heat-activated background K+ channel. EMBO J. *19*, 2483–2491. https://doi.org/10.1093/emboj/19.11.2483.

36. Kang, D., Choe, C., and Kim, D. (2005). Thermosensitivity of the two-pore domain K+ channels TREK-2 and TRAAK. J. Physiol. *564*, 103–116. https://doi.org/10.1113/jphysiol.2004.081059.

37. Sandoz, G., Douguet, D., Chatelain, F., Lazdunski, M., and Lesage, F. (2009). Extracellular acidification exerts opposite actions on TREK1 and TREK2 potassium channels via a single conserved histidine residue. Proc. Natl. Acad. Sci. USA *106*, 14628–14633.

38. Cohen, A., Ben-Abu, Y., Hen, S., and Zilberberg, N. (2008). A Novel Mechanism for Human K2P2.1 Channel Gating. J. Biol. Chem. *283*, 19448–19455. https://doi.org/10.1074/jbc.m801273200.

39. Bagriantsev, S.N., Peyronnet, R., Clark, K.A., Honoré, E., and Minor, D.L. (2011). Multiple modalities converge on a common gate to control K2Pchannel function. EMBO J. *30*, 3594–3606. https://doi.org/10.1038/emboj.2011.230.

40. Ke, R., Ingram, P.J., and Haynes, K. (2013). An integrative model of ion regulation in yeast. PLoS Comput. Biol. *9*, e1002879.

STAR★METHODS

KEY RESOURCES TABLE

REAGENT or RESOURCE	SOURCE	IDENTIFIER
Critical commercial assays		
mMessage mMACHINE T7 Transcription Kit	Thermo Fisher	Cat#AM1344
QuikChange Site-Directed Mutagenesis kit	Stratagene	N/A
Deposited data		
Electrophysiology Data Excel Files	This paper	https://doi.org/10.5061/dryad.t76hdr893
Experimental models: Organisms/strains		
Stage V & VI *Xenopus laevis* oocytes	Xenopus1	xenopus1.com
Recombinant DNA		
CaTOK pMAX plasmid	*Lewis*et al.[3]	N/A
ScTOK pMAX plasmid	*Lewis*et al.[3]	N/A
AfTOK pMAX plasmid	*Lewis*et al.[3]	N/A
CnTOK pMAX plasmid	*Lewis*et al.[3]	N/A
CaTOK-H144K pMAX plasmid	This paper	N/A
CaTOK-H144N pMAX plasmid	This paper	N/A
CaTOK-H144N pMAX plasmid	This paper	N/A
CaTOK-ScTOK C-terminus chimera pMAX plasmid	This paper	N/A
CaTOK-ScTOK chimera 1 pMAX plasmid	This paper	N/A
CaTOK-ScTOK chimera 2 pMAX plasmid	This paper	N/A
CaTOK-P2A pMAX plasmid	This paper	N/A
CaTOK-P2B pMAX plasmid	This paper	N/A
CaTOK-P2C pMAX plasmid	This paper	N/A
CaTOK-K456R pMAX plasmid	This paper	N/A
CaTOK-S458G pMAX plasmid	This paper	N/A
CaTOK-L459A pMAX plasmid	This paper	N/A
CaTOK-V462A pMAX plasmid	This paper	N/A
CaTOK-S466I pMAX plasmid	This paper	N/A
CaTOK-V469L pMAX plasmid	This paper	N/A
CaTOK-H144N, S466I pMAX plasmid	This paper	N/A
CaTOK-H144N, V462A, S466I pMAX plasmid	This paper	N/A
Software and algorithms		
pClamp 9.2	Molecular Devices	moleculardevices.com
Clampfit 11.2	Molecular Devices	moleculardevices.com
GraphPad Prism 10	Prism	www.graphpad.com
Biorender	Biorender	www.biorender.com

EXPERIMENTAL MODEL DETAILS

We used defolliculated stage V and VI *Xenopus laevis* oocytes (Xenoocyte, Dexter, MI, US) for electrophysiological recordings. We incubated the oocytes at 16°C in ND96 oocyte storage solution containing penicillin and streptomycin, with daily washing, for 1 day prior to two-electrode voltage-clamp (TEVC) recording.

METHOD DETAILS

Channel subunit cRNA preparation and Xenopus laevis oocyte injection

We generated cRNA transcripts encoding TOK channels from *Candida albicans*, *Aspergillus fumigatus*, *Cryptococcus neoformans* var. *neoformans*, and *Saccharomyces cerevisiae*, by *in vitro* transcription using the T7 mMessage mMachine kit (Thermo Fisher Scientific), after vector linearization, from cDNA sub-cloned into plasmids (pMAX) incorporating *Xenopus laevis* β-globin 5′ and 3′ UTRs flanking the coding region to enhance translation and cRNA stability. Mutant TOK channel cDNAs were generated by Genscript (Piscataway, NJ, USA) or using QuickChange Site-Directed Mutagenesis kit (Stratagene, La Jolla, CA), and cRNAs made as above. We injected defolliculated stage V and VI *Xenopus laevis* oocytes (Xenoocyte, Dexter, MI, US) with TOK cRNAs (1–5 ng). We incubated the oocytes at 16°C in ND96 oocyte storage solution containing penicillin and streptomycin, with daily washing, for 1 day prior to two-electrode voltage-clamp (TEVC) recording.

Two-electrode voltage clamp (TEVC)

We performed TEVC (Figure 1C) at room temperature using an OC-725C amplifier (Warner Instruments, Hamden, CT) and pClamp10 software (Molecular Devices, Sunnyvale, CA) 1 day after cRNA injection. Oocytes were placed in a small-volume oocyte bath (Warner) and viewed with a dissection microscope. Oocytes expressing TOK channels were recorded in 4 mM extracellular KCl bath solution containing (in mM): 96 NaCl, 4 KCl, 1 $MgCl_2$, 1 $CaCl_2$ unless otherwise indicated. Extracellular 4 mM KCl solutions were buffered (in mM) with: 10 MES (pH 4.0 to 5.5), 10 HEPES (pH 6.0 to 7.5), 5 CHES (pH 8.0 to 9.5). Pipettes were of 1–2 MΩ resistance when filled with 3 M KCl. We recorded currents in response to voltage pulses between −120/-80 mV and +40 mV at 10 mV intervals from a holding potential of −80 mV, to yield current-voltage relationships and examine activation kinetics. We plotted raw or normalized tail currents for CaTOK versus prepulse voltage and fitted with a single Boltzmann function:

$$g = A1 + \frac{(A_2 - A_1)}{\{1+exp\,[V - V_1]/Vs\}} \qquad \text{(Equation 1)}$$

where g is the normalized tail conductance, A_1 is the initial value at $-\infty$ (very negative membrane potential), A_2 is the final value at $+\infty$ (very positive membrane potential), $V_{1/2}$ is the half-maximal voltage of activation and V_s the slope factor. We analyzed data using Clampfit (Molecular Devices) and Graphpad Prism software (GraphPad, San Diego, CA, USA), stating values as mean ± SEM.

Relative permeability calculations

The Goldman-Hodgkin-Katz (GHK) equation states:

$$V_m = \frac{RT}{ZF} \ln P_k[K^+]_O + P_{Na}[Na^+]_O + P_{cl}[Cl^-]_i \Big/ P_k[K^+]_i + P_{Na}[Na^+]_i + P_{Cl}[Cl^-]_O \qquad \text{(Equation 2)}$$

Where V_m is the absolute reversal potential and P is the permeability. By knowing the intracellular and extracellular concentrations of each ion, one can modify this equation to calculate the relative permeability of each ion. Here, we modified the equation to determine the relative permeability of two ions in a system in which only the extracellular ion concentration was known. By plotting the I/V relationships for CaTOK in the presence of 100 mM Rb^+, Na^+, and Cs^+ we can compare their relative permeability to 100 mM K^+. Permeability ratios for each ion (x) compared to K^+ were calculated as,

$$\Delta E_{REV} = E_{REV,x} - E_{REV,K} = \frac{RT}{ZF} \ln \frac{P_x}{P_k} \qquad \text{(Equation 3)}$$

CaTOK structure prediction

We used AlphaFold[13,14] to generate a predicted structure for CaTOK. We visualized the CaTOK channel structure in UCSF Chimera,[15] which we also used to generate figures.

QUANTIFICATION AND STATISTICAL ANALYSIS

All values are expressed as mean ± SEM. Comparison of two groups was conducted using a t-test; all p values were two-sided. One-way ANOVA was applied to all tests comparing more than two groups; all p values were two-sided. Individual statistical details for each experiment are shown in figure legends.